



NJC

**Effect of Ligand Substituents on Nickel and Copper [N4]
Complexes: Electronic and Redox Behavior, and Reactivity
towards Protons**

Journal:	<i>New Journal of Chemistry</i>
Manuscript ID	NJ-ART-03-2019-001283.R1
Article Type:	Paper
Date Submitted by the Author:	21-Jun-2019
Complete List of Authors:	Kankanamalage, Pavithra ; Wayne State University, Chemistry Ekanayake, Danushka; Wayne State University, Chemistry Singh, Nirupama; University of Alabama in Huntsville, Department of Chemistry de Morais, Ana Carolina; Universidade Federal Fluminense, Inorganic Chemistry Mazumder , Shivnath; Wayne State University, Chemistry Verani, Claudio; Wayne State University, Chemistry Mukherjee, Anusree; University of Alabama in Huntsville, Department of Chemistry Lanznaster, Mauricio; Universidade Federal Fluminense, Inorganic Chemistry

SCHOLARONE™
Manuscripts

Effect of Ligand Substituents on Nickel and Copper [N₄] Complexes: Electronic and Redox Behavior, and Reactivity towards Protons

Pavithra H. A. Kankanamalage,^{[a],†} Danushka M. Ekanayake,^{[a],†} Nirupama Singh,^{[b],‡} Ana C. P. de Morais,^{[c],‡} Shivnath Mazumder,^{[d],*} Cláudio N. Verani^{[a],*}, Anusree Mukherjee,^{[b],*} Mauricio Lanznaster,^{[c],*}

[a] Department of Chemistry, Wayne State University, Detroit, MI 48202, USA. E-mail: claudio.verani@wayne.edu

[b] Department of Chemistry, University of Alabama, Huntsville, AL 35899, USA. E-mail: am0095@uah.edu

[c] Instituto de Química, Universidade Federal Fluminense, 24020-141, Niterói, RJ, Brazil. E-mail: ml@id.uff.br

[d] Department of Chemistry, Indian Institute of Technology Jammu, Jammu (J&K) -181221, India
Email: shivnath.mazumder@iitjammu.ac.in

†, ‡ Authors contributed equally to the manuscript

Abstract

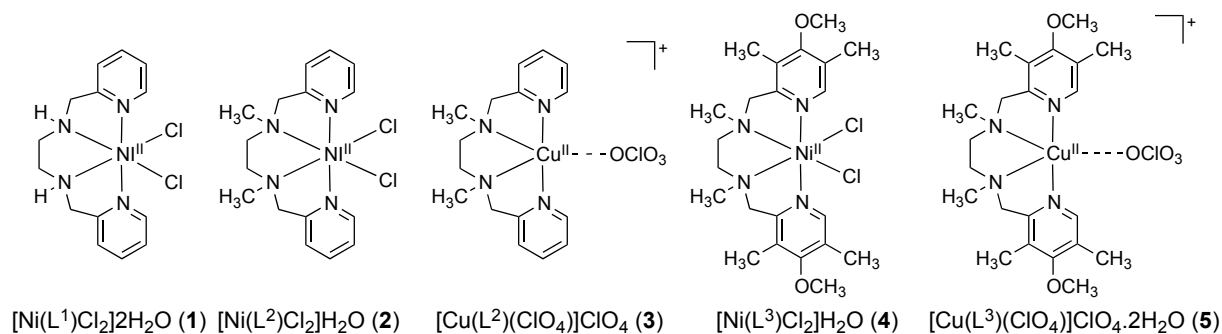
This paper describes the synthesis, electronic and redox properties of three nickel(II) and two copper(II) complexes, namely, [Ni(L¹)(Cl)₂].2H₂O (**1**), [Ni(L²)(Cl)₂].H₂O (**2**), [Cu(L²)(ClO₄)]ClO₄ (**3**), [Ni(L³)(Cl)₂].H₂O (**4**), and [Cu(L³)(ClO₄)]ClO₄.2H₂O (**5**). Ligands L¹, L² and L³ respectively contain a 1,2-bis((pyridine-2-ylmethyl)-azaneyl)ethane framework decorated with electron donating methyl and methyl/methoxy substituents. We observe a correlation between electron donating capability of the ligands (L¹ < L² < L³) and the redox potential for the M^{II}/M^I couple (**1** > **2** > **4** and **3** > **5**). After thorough identification of the spectroscopic and redox properties of **1** – **5**, the reactivity of the complexes was investigated towards proton and water reduction by means of electro and photocatalysis. These species seemingly support H₂ evolution and display tunable catalytic properties achieved through the presence of differentiated electron donicity. Evidence of degradation with nanoparticle conversion was found to depend on the nature of both ancillary ligand and metal center.

Introduction

Coordination complexes containing 3d metal ions display rich redox and spectroscopic behavior that is versatile on oxidation numbers and on ligand fields. These complexes offer the opportunity to use such properties in order to tune specific reactivities that may allow for their use as molecular catalysts. Therefore, when compared to heterogeneous materials,⁷ 3d-based molecular catalysts become very relevant for their unsurpassed tenability. Furthermore, they also present themselves as affordable alternatives to less abundant 4d and 5d congeners in catalytic reactions such as H₂ formation from water or protons.¹⁻⁶ Cobalt, nickel and copper complexes are of special interest for hydrogen evolution reactions (HER), because they display accessible low oxidation states required during the catalytic cycle.⁷⁻¹⁶ The general mechanism of H₂ production involves a one-electron reduction from M^{II} to M^I, followed by the transfer of two electrons to a H⁺ to form a M^{III}-H⁻ hydride species. Upon an additional one-electron reduction, a M^{II}-H⁻ species is generated, which finally interacts with another H⁺ to yield H₂, while the M^{II} catalyst is regenerated.⁸⁻¹⁶ Nonetheless, reaching the energetically demanding M^{III} oxidation state in nickel and copper catalysts is questionable, and the reduction of [M^{II}(L)] to [M^I(L)] and to [M⁰(L)] or [M^I(L^{*})] is equally accessible.¹⁷⁻²²

The nature of the ligands play a major role in a catalyst performance, as accessibility of intermediates with different oxidation state might be preferred with certain ligand systems. Coordination number, nature of the donor atoms (N, O, S, P), size and number of chelate rings and the presence of electron-donor/acceptor substituents are among the main parameters that can be easily modified in a catalyst to achieve water solubility, robustness and high efficiencies required for HER. So far, a number of five-coordinate catalysts of cobalt, nickel and copper with N,O-donor ligands has been investigated.^{3,19-25} It is expected that the chelate effect of such ligands minimizes degradation, while a 'free' coordination position is available for substrate binding. Despite several important accomplishments, most catalysts lack solubility, lose efficiency, or decompose in water.

On the other hand, nickel and copper complexes with four-coordinate ligands are less common in HER investigations.^{9,16,26,27} Here, we describe a series of three nickel complexes, $[\text{Ni}(\text{L}^1)(\text{Cl})_2] \cdot 2\text{H}_2\text{O}$ (**1**), $[\text{Ni}(\text{L}^2)(\text{Cl})_2] \cdot \text{H}_2\text{O}$ (**2**), and $[\text{Ni}(\text{L}^3)(\text{Cl})_2] \cdot \text{H}_2\text{O}$ (**4**), and two copper complexes, $[\text{Cu}(\text{L}^2)(\text{ClO}_4)]\text{ClO}_4$ (**3**) and $[\text{Cu}(\text{L}^3)(\text{ClO}_4)]\text{ClO}_4 \cdot 2\text{H}_2\text{O}$ (**5**), with the 1,2-bis((pyridine-2-ylmethyl)-azaneyl)ethane framework (L^1) and the equivalent counterparts containing methyl (L^2) and methyl/methoxy (L^3) substituents (**Scheme 1**). The methyl and methoxide substituents have an inductive electron donor effect, which is expected to increase the electron donating ability of the ligands in the order: $\text{L}^1 < \text{L}^2 < \text{L}^3$.²⁸⁻³⁰ Thus, the effects of the ligands on electron density of the metal center, the redox behavior and reactivity of the complexes towards HER were investigated.



Scheme 1. Illustration of the $3d^8$ nickel(II) and $3d^9$ copper(II) complexes **1-5**.

Results and Discussion

Synthesis and characterization

Ligands L^1 and L^2 were obtained by previously described procedures,³¹⁻³³ while L^3 was synthesized by treatment of *N,N'*-dimethylethylenediamine with 2-chloromethyl-4-methoxy-3,5-dimethylpyridine hydrochloride in dichloromethane. Complex $[\text{Ni}(\text{L}^1)\text{Cl}_2] \cdot 2\text{H}_2\text{O}$ (**1**) was synthesized by treating L^1 with $[\text{Ni}(\text{H}_2\text{O})_6]\text{Cl}_2$ in ethanol and the product was crystallized using diethyl ether vapor diffusion. Complexes $[\text{Ni}(\text{L}^2)\text{Cl}_2] \cdot \text{H}_2\text{O}$ (**2**) and $[\text{Cu}(\text{L}^2)\text{ClO}_4] \cdot \text{ClO}_4$ (**3**) were synthesized by reported procedures.³¹ Complex $[\text{Ni}(\text{L}^3)\text{Cl}_2] \cdot \text{H}_2\text{O}$ (**4**) and $[\text{Cu}(\text{L}^2)\text{ClO}_4] \cdot \text{ClO}_4 \cdot 2\text{H}_2\text{O}$ (**5**) were synthesized by adding ligand L^3 to a solution of $[\text{Ni}(\text{H}_2\text{O})_6]\text{Cl}_2$ and $[\text{Cu}(\text{H}_2\text{O})_6](\text{ClO}_4)_2$ in methanol respectively. The complexes were characterized spectroscopically by FTIR and $^1\text{H-NMR}$ methods, as well as by elemental analysis and electron spray ionization mass spectrometry (ESI-MS). The ESI-MS spectra of complexes **1**, **2**, and **4** in MeOH showed m/z^+ peaks at 335.0, 363.2, and 479.3, respectively, for $[\text{Ni}(\text{L}^1)(\text{Cl})]^+$, $[\text{Ni}(\text{L}^2)(\text{Cl})]^+$, and $[\text{Ni}(\text{L}^3)(\text{Cl})]^+$. For complexes **3** and **5**, the m/z^+ peaks in MeOH were observed at 432.1 and 548.2 for the species $[\text{Cu}(\text{L}^2)(\text{ClO}_4)]^+$ and $[\text{Cu}(\text{L}^3)(\text{ClO}_4)]^+$, respectively. The NMR spectra of complexes **1**, **2**, and **4** displayed broad peaks associated with paramagnetic species; hence they are not square planar in geometry. The crystal structures of complex **2** and **3** were described elsewhere,^{31,34} The structure of **2** was solved by the late Ribak-Akimova³⁴ and revealed the nickel center coordinated to L^3 and two chloride anions in a distorted octahedral geometry. The two chloro atoms are *cis* to each other and

trans to the ethane-1,2-diamine nitrogen atoms, while the two pyridine rings are mutually *trans*. One water molecule was found in the second coordination sphere. Complex **3** was solved by one of us³¹ and shows a copper center in a distorted square-pyramidal geometry ($\tau = 0.35$), with four nitrogen atoms of L² in the base of the pyramid and one oxygen atom from a weakly coordinated perchlorate counterion in the axial site (Cu-O, 2.2459 Å). Repeated attempts to obtain X-ray suitable single crystals for complexes **1**, **4** and **5** have been unsuccessful.

Electronic and electrochemical properties

The electronic absorption spectra of **1**, **2**, and **4** were recorded in MeOH due to the limited solubility in MeCN (Table 1, Figures 1, S1, S2 and S4). The complexes show a pronounced band at 263 nm ($\epsilon \approx 5600 - 8300 \text{ M}^{-1}\text{cm}^{-1}$) due to intraligand charge transfer. The molar absorptivity of this band increases with the electron donating ability of the ligand with no change of the wavelength.

Table 1. UV-visible spectroscopic data for **1-5**.

Complex	λ_{max} , nm / (ϵ , $\text{M}^{-1} \text{cm}^{-1}$)
1 ^a	263 (5689), 309 (133), 578 (7), 948 (13)
2 ^a	263 (6600), 300 (202), 601 (7), 988 (12)
3 ^b	262 (10500), 283 (4700), 620 (240)
4 ^a	263 (8266), 612 (6), 988 (12)
5 ^b	262 (11616), 285 (5700), 620 (258)

(a) In methanol; (b) in acetonitrile

Complexes **1** and **2** show an extra intraligand charge transfer band at $\approx 300 \text{ nm}$ ($\epsilon \approx 130 - 200 \text{ M}^{-1}\text{cm}^{-1}$) compared to **4**. For **1**, the absorption at $\approx 300 \text{ nm}$ appears as a well-defined band, while a shoulder is observed for **2**. Although complexes **1**, **2**, and **4** do not show obvious metal/ligand CT bands, two low-intensity d-d transitions are observed at $\approx 600 \text{ nm}$ ($\epsilon \approx 7$, ${}^3\text{T}_2 \leftarrow {}^3\text{A}_2$) and $\approx 950 \text{ nm}$ ($\epsilon \approx 12$, ${}^3\text{T}_1(\text{F}) \leftarrow {}^3\text{A}_2$).³⁶ As a consequence of an increasing electron donating ability, the d-d bands for complex **1** at ≈ 600 and $\approx 950 \text{ nm}$ are red shifted to ≈ 610 and 990 nm , respectively in **2** and **4**. Because the latter complexes show similar shifts, it is possible to conclude that the most relevant way to affect such change is by functionalizing the amine nitrogen atoms, leading to destabilization of the d π -orbitals.

^{31,34,37}

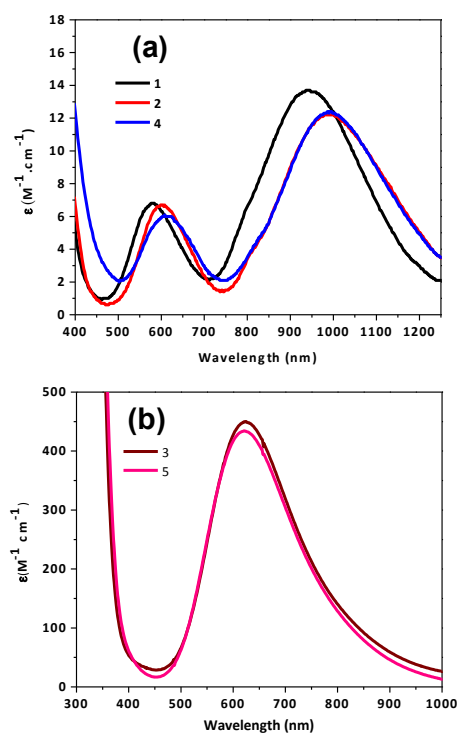


Figure 1. UV-visible spectra of the complexes showing d-d transitions: (a) Complexes **1**, **2**, and **4** (MeOH, 1×10^{-2} M); (b) Complexes **3** and **5** (MeCN, 2×10^{-3} M).

The UV-visible spectra of complexes **3** and **5** were recorded in MeCN (Figures 1, S3 and S5) and show a prominent band at 262 nm ($\epsilon \approx 10500 - 11600 \text{ M}^{-1}\text{cm}^{-1}$), which can be assigned to an intraligand charge transfer. The molar absorptivity of this band increases with the electron donating ability of the ligand. Another intraligand band appears as a shoulder at 285 nm ($\epsilon \approx 4750\text{-}5580 \text{ M}^{-1}\text{cm}^{-1}$) for both complexes. The weak broad absorption observed at 620 nm ($\epsilon \approx 260 \text{ M}^{-1}\text{cm}^{-1}$) in **3** and **5** is attributed to d-d transitions of the $3d^9 \text{Cu(II)}$ center.³⁸

To understand the effect of the electron donating groups on the redox activity of the complexes, cyclic voltammograms were taken in MeCN (Figure S6, Table 2). Complexes **1**, **2**, and **4** exhibited reduction waves at -1920 , -2000 , and $-2170 \text{ mV}_{\text{Fc}/\text{Fc}^+}$ respectively, assigned to $\text{Ni}^{\text{II}}/\text{Ni}^{\text{I}}$ reduction.^{3,39} These potentials suggest that the more electron donating the ligand is, more negative the potential of the $\text{Ni}^{\text{II}}/\text{Ni}^{\text{I}}$ couple will be.²⁴ Therefore, the $\text{Ni}^{\text{II}}/\text{Ni}^{\text{I}}$ process becomes harder to achieve in the order: **1** < **2** < **4**.^{40,41} A similar trend was observed for the $\text{Cu}^{\text{II}}/\text{Cu}^{\text{I}}$ processes, in which the $E_{1/2}$ of **3** appears at $-480 \text{ mV}_{\text{Fc}/\text{Fc}^+}$, whereas the $E_{1/2}$ of **5** appears at $-550 \text{ mV}_{\text{Fc}/\text{Fc}^+}$. Likewise, as the electron donating capability of the ligands increases, the potential for the $\text{Ni}^{\text{II}}/\text{Ni}^{\text{III}}$ couple is expected to decrease. The processes associated with the $\text{Ni}^{\text{II}}/\text{Ni}^{\text{III}}$ oxidation were observed at 730 , 640 , and $700 \text{ mV}_{\text{Fc}/\text{Fc}^+}$ for complexes **1**, **2**, and **4**.⁴² As expected, the potential for $\text{Ni}^{\text{II}}/\text{Ni}^{\text{III}}$ oxidation decreases from complex **1** to **2**. Nonetheless, from complex **2** to **4**, the potential increases. This result suggests that the $p\text{-OCH}_3/(m\text{-CH}_3)_2$ substituents in the pyridines have a different impact on the oxidation potential of nominal $\text{Ni}^{\text{II}}/\text{Ni}^{\text{III}}$. Studies show that electron donating groups on the *para* position of the pyridine in polypyridine ligand systems are capable of lowering the $\text{M}^{\text{II}}/\text{M}^{\text{III}}$ oxidation potential.^{41,43} However, the *m*-methyl substituents in **4** can increase the oxidation potential of the $\text{M}^{\text{II}}/\text{M}^{\text{III}}$ process due to steric constraints.⁴⁴⁻⁴⁶ Thus, it is possible that the steric effect of the *meta*-substituted methyl groups partially neutralizes the electron donating effect of OMe groups at the *para* position of the pyridine arms. An opposite effect has also been observed for cobalt and iron complexes with L^1 and L^2 . The $\text{M}^{\text{III}}/\text{M}^{\text{II}}$ potential became more positive for the complexes with the methylated L^2 ligand, which has been assigned to the steric

constraints caused by the CH₃ groups.⁴⁷⁻⁴⁹ In contrast to the nickel complexes, oxidation processes associated with the Cu^{II}/Cu^{III} couple could not be observed in the CVs of complexes **3** and **5**.

Table 2. Cyclic voltammetric data for complexes **1-5** in MeCN.

Complex	M ^(III/II) /mV _{Fc/Fc⁺}	M ^(II/I) / mV _{Fc/Fc⁺}
1	E _{pa} = 730	E _{pc} = -1930
2	E _{pa} = 640	E _{pc} = -2000
3	---	E _{1/2} = -480; ΔE = 70 ; i _{pc} /i _{pa} = 0.42
4	E _{pa} = 700	E _{pc} = -2170
5	---	E _{1/2} = -550; ΔE = 110 ; i _{pc} /i _{pa} = 0.43

Reactivity Studies

Electrocatalytic proton reduction: The catalytic activity of **1-5** was probed by cyclic voltammetry in MeCN, in the presence of 0 to 10 equivalents of acetic acid as the proton source (Figure S7). For complexes **1**, **2**, and **4**, the current associated with the Ni^{II}/Ni^I couple increases with the increasing amounts of acid. This behavior suggests that catalysis is related to the Ni^{II}/Ni^I reduction process. Controlled experiments in the absence of the complexes (Figure S8) produced negligible catalytic peaks at more negative potentials, validating the catalytic activity of the Ni^I species. To support the association between the catalytic peaks in the voltammograms and the H₂ production, bulk electrolysis (BE) experiments were performed with 100 equivalents of acetic acid, using a Hg pool working electrode (WE) at an applied potential of -1700 mV_{Ag/AgCl} in MeCN. For complexes **1**, **2**, and **4**, turnover numbers (TON) of 12, 10, and 4.5 were achieved with Faradaic efficiencies (% FE) of 81, 34, and 38 %, respectively, after 3 h catalysis (Figure 2). These results indicate a correlation between the Ni^{II}/Ni^I reduction process, TONs and Faradaic efficiencies. In other words, the increasing electron-donating capability of the ligands leads to more negative potentials, which lower TONs and Faradaic efficiencies. For the copper complexes **3** and **5**, an increase in catalytic current after a successive addition of acid aliquots was also observed, but at more negative potentials (≈ 2200 mV_{Fc/Fc⁺}). The increasing current of multiple reduction processes (Figure S7) suggest that ligand-based redox processes may be involved.²¹ Bulk electrolysis for **3** and **5** yielded TONs of 4 and 3 with faradaic efficiencies of 32 and 27 % respectively. Despite the differences in electron-donating capabilities of L² and L³, the catalytic activity of both complexes is similar, suggesting the generation of ligand-based radicals that lead to catalyst deactivation under acidic conditions.

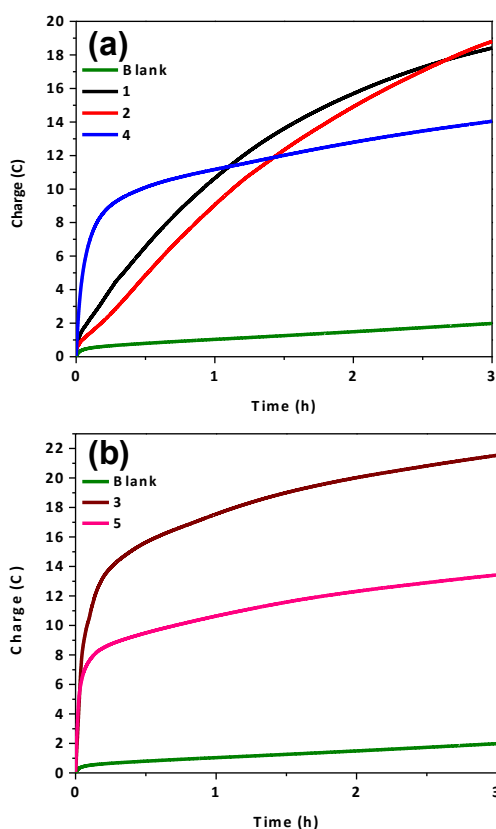


Figure 2. Charge vs. time plot for 3 h BE in MeCN at $-1700 \text{ mV}_{\text{Ag}/\text{AgCl}}$ (a) for complexes **1**, **2**, and **4**; (b) for complexes **3** and **5**. Catalyst ($5 \times 10^{-6} \text{ mol}$), acetic acid (100 equivalents), electrodes: Hg pool (WE), Ag/AgCl (RE), Pt wire (AE).

Electrocatalytic water reduction: The activity of complexes **1-5** as potential catalysts for water reduction was evaluated by CV experiments in phosphate buffer (1 M, pH 7) using a mercury pool working electrode.^{20,21} In the absence of the complexes, H_2 was generated at $-1850 \text{ mV}_{\text{Ag}/\text{AgCl}}$. In the presence of the nickel complexes, the peak associated with the H_2 production shifted anodically to -1500 , -1550 , and $-1600 \text{ mV}_{\text{Ag}/\text{AgCl}}$ (**Figure 3a**), respectively for **1**, **3**, and **4**. Thus, these complexes are catalytic towards water reduction, with onset overpotentials of 880, 930, and 980 mV. It seems that the cathodic shift of the catalytic peaks correlates with the $\text{Ni}^{\text{II}}/\text{Ni}^{\text{I}}$ reduction potentials, which is associated with the increasing electron donating capability of the ligands in **1**, **3**, and **4**. For the copper complexes, the catalytic peak shifted to -1520 and $-1600 \text{ mV}_{\text{Ag}/\text{AgCl}}$ with onset overpotentials of 900 and 980 mV for **3** and **5**, respectively (**Figure 3b**). The thermodynamic potential for H^+ to H_2 was taken as $-617 \text{ mV}_{\text{Ag}/\text{AgCl}}$ in pH 7 aqueous solution.⁵⁰ In order to confirm the onset overpotential, BE experiments were performed in phosphate buffer (1 M, pH 7) with a mercury pool working electrode. During the experiments, overpotentials varying from 180 mV to 1200 mV were applied for three minutes at each interval. Negligible charge consumptions were measured for complexes **1-5** below 780, 830, 880, 980, and 930 mV, respectively (Figures S9-S13). Thus, the onset overpotential for the nickel complexes is 783 mV for **1**, 830 mV for **2** and 980 mV for **4**. For the copper complexes, the onset overpotential is 880 mV for **3** and 930 mV for **5**. According to these results, a stronger electron donating capability of the ligand leads to a higher onset overpotential.

To confirm that the catalytic peaks observed in the cyclic voltammograms (Figure 3) are associated with the reduction of water to H_2 , BE experiments were performed at $-1700 \text{ mV}_{\text{Ag}/\text{AgCl}}$ in phosphate buffer (1 M, pH 7). Under these conditions, the nickel complexes **1**, **2**, and **4** gave TONs of 950, 528, and 147 with Faradaic efficiencies of 96, 82, and 82 %, respectively, after 3 h of catalysis (Figure 4a). Under the same conditions, the copper complexes yielded TONs of 840 and 230 with Faradaic efficiencies of 72 and 64 % for **3** and **5**, respectively (Figure 4b). UV-visible absorption spectra recorded before and after catalysis (Figure S14) revealed that a significant change in the spectral

features was observed for complexes **1**, **2**, **3** and **5**, suggesting that decomposition takes place during the catalytic cycle. These changes were not observed for complex **4**.

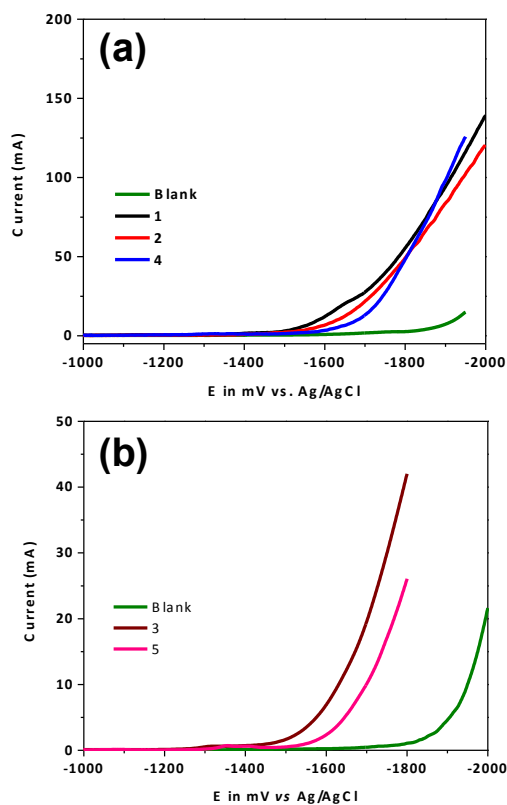


Figure 3. Cyclic voltammograms of the complexes in water (pH 7, 1 M phosphate buffer); (a) For complexes **1**, **2**, and **4**. (b) For complexes **3** and **5**.

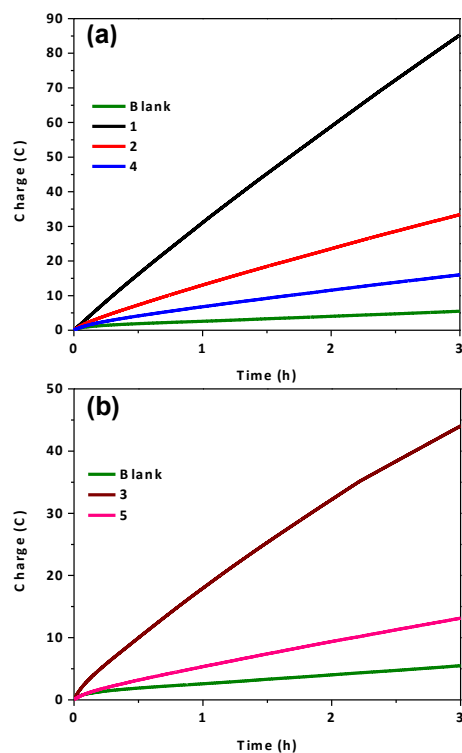


Figure 4. Charge vs. time plot for 3 h BE in phosphate buffer (pH 7) at $-1700 \text{ mV}_{\text{Ag/AgCl}}$ (a) for complexes **1**, **2** and **4**. (b) for complexes **3** and **5**. Catalyst ($0.2 \times 10^{-6} \text{ mol}$), Electrodes: Hg pool (W), Ag/AgCl (R), Pt wire (A).

Photocatalytic water reduction: Complexes **1-5** were tested for hydrogen generation in water/EtOH (1:1) at pH \approx 12, using green light (520 nm), fluorescein (1×10^{-3} M) as the photosensitizer and triethylamine (TEA 5 % v/v) as the sacrificial electron donor.²⁰ The nickel complexes yielded turnover numbers of 310 for **1**, 365 for **2** and 196 for **4**, while the copper complexes **3** and **5** yielded TONs of 128 and 98, respectively, in a 24 h period. The pH variations from 10 to 13 revealed an optimal performance at pH 11 for **1**, **3** and **5** and at pH 12 for **2** and **4**. The influence of the catalyst concentration ($1 - 30 \times 10^{-6}$ M) on photocatalysis was evaluated for the nickel complexes using fluorescein (1×10^{-3} M) and TEA (5% v/v) constant concentrations in water/EtOH (1:1) at pH 11 for complex **1** and pH 12 for complexes **2** and **4**. The higher TONs (5640 for **1**, 5120 for **2**, and 4970 for **4**, in 24 h) were observed for the lowest concentration of the catalyst (1×10^{-6} M) (Figure 5a). Similar behavior was observed for the Cu complexes when the concentration varied from $5 - 60 \times 10^{-6}$ M, yielding TONs of \approx 1000 in 24 h for both **3** and **5** (Figure 5b). As observed previously for the electrocatalysis experiments, a correlation between the TONs and the electron donating capability of the ligands was observed for the nickel but not for the copper complexes.

Decomposition of the catalysts during the photocatalysis experiments to form metal colloid was evaluated by adding 0.1 mL of elemental mercury to the reaction vessel.⁵¹ It has been established that nanoparticles lose catalytic activity via Hg poisoning. As such, if the catalysis is molecular no change should be observed in presence of Hg. On the other hand, if catalytic activity is solely due to active nanoparticles, generation of hydrogen should cease upon addition of the metal. Interestingly, the catalytic activity of **1** and **2** has decreased to \sim 50%, while that of **4** decreased only marginally (\sim 10%). Decomposition of **1** and **2** takes place during the catalytic cycle (see UV-visible data on Figure S14). This decomposition is likely linked to the formation of nanoparticles that get deactivated in presence of Hg. Compound **4** seems to be a genuine molecular catalyst.

These results indicate that partial catalyst conversion takes place. Nonetheless, the continued catalytic activity in the presence of elemental mercury suggests that molecular-based photoconversion of water into dihydrogen takes place in some extent. In contrast to the nickel complexes, no hydrogen generation was observed for complexes **3** and **5** in the presence of Hg, which indicates that copper metal particles are the catalytic active species.

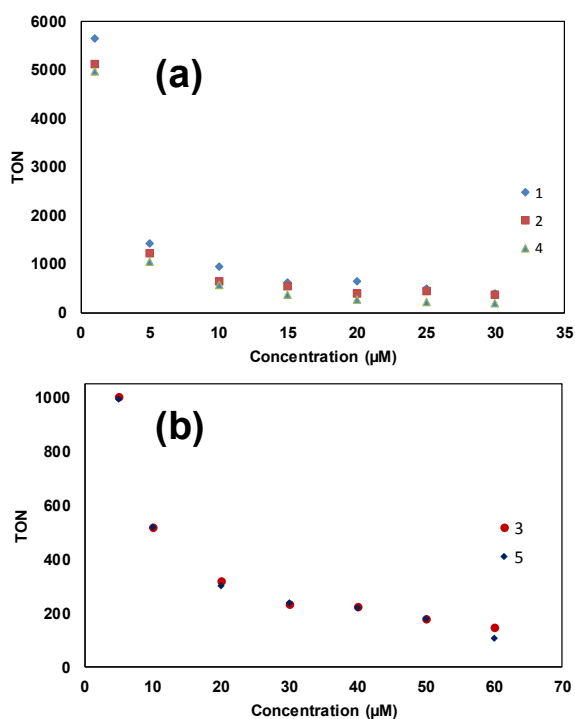


Figure 5. Variation of the photocatalytic TONs with concentration for **1-5**.

Density Functional Theory Evaluation of Decomposition Pathways: The catalysts were investigated by DFT calculations. The B3LYP density functional was used as it provides reliable results for 3d metal-containing water/proton reduction catalysts.^{11, 12, 20, 21} In addition, the B3LYP-calculated structures for **2** and **3** match nicely with the available crystallographic structures (Tables S1 and S2). For complex **3** shown in Figure 6 a four-coordinate Cu^{II} center was used as a simplified model. Upon 1-electron reduction, the Cu^I species **3A** is generated with Cu-L bond distances significantly elongated (Cu-N2 = 2.53 Å and Cu-N3 = 3.36 Å). Additionally the N1-Cu-N4 angle becomes highly distorted (157.7°) in **3A**. Solvation and dissociation of the ligand L² might follow to form a pseudo-tetrahedral **3B** species. As shown in Figure 6, this process is energetically accessible. The Cu^I species, obtained from the reduction of Cu^{II} in water, can also disproportionate to Cu⁰ and agglomerate to form nanoparticles, leading to the decomposition of the molecular catalyst.

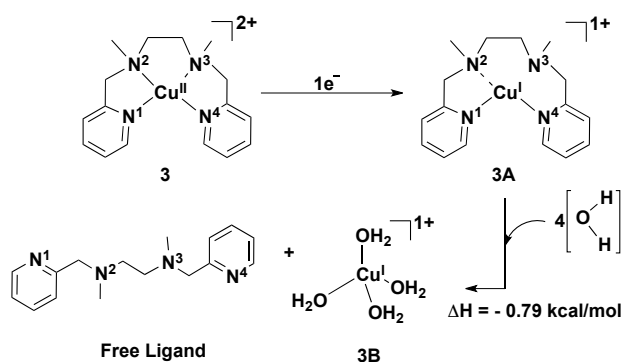


Figure 6. DFT calculated mechanistic pathway for the decomposition of Cu catalyst **3** in water.

The decomposition pathway for **1** is depicted in Figure 7. The calculated results indicate that the high spin Ni^{II} catalyst can undergo a one-electron reduction at $-2.43 \text{ V}_{\text{Fc}/\text{Fc}^+}$. The loss of chlorides in the Ni^I complex is thermodynamically favored by $\Delta G = 30 \text{ kcal/mol}$. For the resulting complex **1B**, a pyridine-Ni bond breaks and a water molecule coordinates to the nickel center, giving rise to **1C**. This process is accessible at room temperature and energetically uphill by only $\Delta G \approx 7 \text{ kcal/mol}$. Therefore, a significant concentration of **1C** may be present in the reaction mixture. The formation of a hydrogen bond with the coordinated water molecule in **1C** may facilitate the reduction of the uncoordinated pyridine at a potential of $-2.35 \text{ V}_{\text{Fc}/\text{Fc}^+}$. Then, the electron rich uncoordinated pyridine can accept a proton from the coordinated water molecule to generate **1D**, which is unproductive for hydrogen evolution.

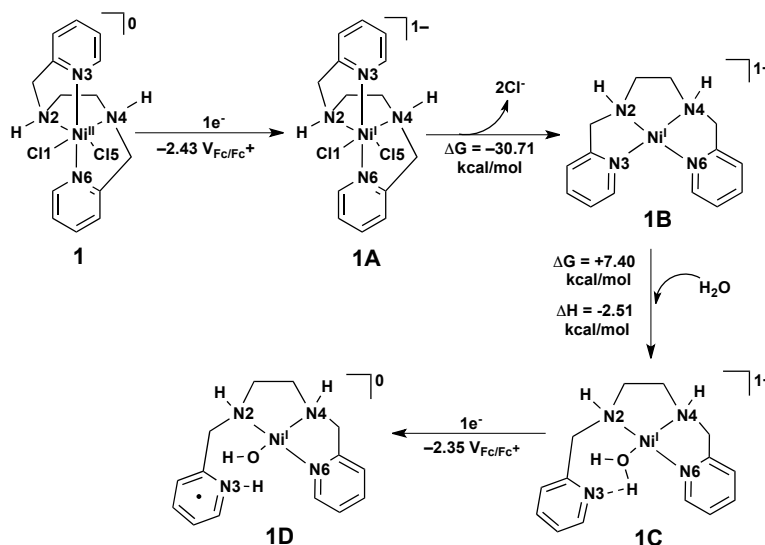


Figure 7. DFT calculated deactivation pathway for the Ni complex **1** in water.

Conclusions

This study evaluates the effect of electron donating groups on the spectroscopic, redox behavior, and reactivity of nickel and copper complexes. The ligand design was chosen in order to identify the peculiarities of four-coordinated systems that are water-soluble. The redox potential for the M^{II}/M^I process became more negative, as a consequence of an increasing electron donating capability of the ligands ($L^1 < L^2 < L^3$). The reactivity of the complexes acting as catalysts in proton and water reduction also reflected the variations in electron density. In the electrocatalytic proton reduction experiments, the TONs of the nickel complexes decreased with the increasing electron donating capability of the ligands. Interestingly, ligand variation did not have the same effect on the copper complexes; this may be associated with the deactivation of the catalysts under acidic conditions. The potential of the catalytic peak, and thus the onset overpotential in the electrocatalytic water reduction experiments also became more negative with the increasing electron donating capabilities of the ligands for both nickel and copper complexes. In these experiments, both TON values decreased in the order **1** > **2** > **4** and **3** > **5**. During photocatalytic water reduction, the TONs decreased with an increase of the catalyst concentration for both nickel and copper complexes. Moreover, the TON values only correlate with the electron donating effect of the ligands for the nickel complexes (TON: **1** > **2** > **4**), and at the lowest concentrations of the complex. Thus, these results suggest that catalyst deactivation is also concentration-dependent. In fact, the addition of Hg to the BE experiments revealed a decrease in the catalytic activity of **1** and **2** by ca. 50 % indicating that both molecular and nanoparticle H_2 generation are operational. For compound **4**, however, Hg poisoning led to negligible deactivation fully supporting molecular-based catalysis. This result shows that deactivation and decomposition of molecular catalysts can be mitigated by means of appropriate tuning of the electronic and steric properties of the ligand. For the copper complexes, H_2 evolution was not observed in the presence of Hg, suggesting that copper particles are the catalytically active species in the photocatalytic water reduction experiments. These results provided strong evidence that ligand functionalization affects efficiency and robustness of the catalysts.

Experimental Section

General. Reagents and solvents were used as received from commercial sources. 1H -NMR spectra were recorded in a Mercury FT-NMR 400 MHz instrument using $CDCl_3$ or CD_3CN as the solvent. Electron spray ionization mass spectrometry (ESI-MS) data was obtained in a triple quadrupole Micromass Quattro LC equipment. The elemental analysis (C, H, and N) was performed using an Exeter analytical CHN analyzer by Midwest Microlab, Indianapolis, IN, USA. UV-visible spectra were recorded in acetonitrile, methanol or pH 7 phosphate buffer solutions and obtained in a Varian Cary 50 spectrophotometer in the range of 200 to 1650 nm with quartz cells at room temperature. Values of ϵ are given in $M^{-1} cm^{-1}$.

Synthesis

Synthesis of the ligands: Ligands L^1 and L^2 were reported elsewhere and synthesized accordingly.³¹⁻³³ Ligand L^3 was synthesized by following a similar route. A solution of potassium carbonate (2.55 g, 18.4 mmol) in water (10 mL) was added dropwise to a solution of 2-chloromethyl-4-methoxy-3,5-dimethylpyridine hydrochloride 2.03 g (9.15 mmol) in 10 mL of water. Addition of potassium carbonate resulted in the formation of a very thick white precipitate. More water (50 mL) was added into the reaction mixture that was stirred at room temperature for additional 30 minutes. Then, the product was extracted with dichloromethane (3×20 mL). The combined dichloromethane layer was treated

with anhydrous sodium sulfate, filtered and the solvent was removed by rotary evaporation. The collected light brown oil was dissolved in dichloromethane (10 mL). The 2-(chloromethyl)-3,4-dimethoxypyridine solution in dichloromethane was added dropwise to a solution of *N,N'*-dimethylethylenediamine 0.471 mL (5.34×10^{-3} mol) in the same solvent (15 mL). An aqueous solution of 1 M sodium hydroxide (10 mL) was slowly added into the solution and stirred for an additional 60 h at room temperature. After 60 h of stirring followed by the rapid addition of a second fraction of aqueous 1 M sodium hydroxide (10 mL, 1×10^{-2} mol), the product was extracted with dichloromethane (3×25 mL). The combined organic layers were dried over anhydrous sodium sulfate and filtered. The excess solvent was evaporated under vacuum to afford a brown colored viscous oil (yield: 1.84 g, 89 %). ^1H NMR (500 MHz, Methanol- d_4) δ 8.10 (s, 2H, pyridine ring), 3.78 (s, 6H, -O-CH₃-Py), 3.59 (s, 4H, benzylic -CH₂-Py), 2.57 (s, 4H, -CH₂-CH₂-), 2.28 (s, 6H, CH₃-Py), 2.24 (s, 6H, CH₃-Py), 2.17 (s, 6H, N-CH₃); ^{13}C NMR (126 MHz, Methanol- d_4) δ 164.81 (s, pyridine), 156.38 (s, pyridine), 147.27 (s, C-H pyridine), 126.89 (s, pyridine), 125.84 (s, pyridine), 61.67 (s, N-CH₂-Py), 59.03 (s, Py-O-CH₃) 55.06 (s, -CH₂-CH₂-), 41.56 (s, N-CH₃) 11.92 (s, CH₃-Py), 9.87 (s, CH₃-Py)

Synthesis of the metal complexes: $[\text{Ni}(\text{L}^1)(\text{Cl})_2] \cdot 2\text{H}_2\text{O}$ (**1**) was synthesized with a slight modification of a reported procedure.³⁴ A solution of $[\text{Ni}^{\text{II}}(\text{H}_2\text{O})_6]\text{Cl}_2$ (0.12 g; 0.50 mmol) in ethanol (2 mL) was heated to 70°C for 15 min and added to the solution of L^1 (0.12 g; 0.50 mmol) in ethanol (2 mL). The resulting blue solution was cooled to room temperature and slow evaporation with diethyl ether yielded blue color crystals (yield: 60%). ESI-MS in MeOH: $m/z^+ = 335.0$ for $[\text{Ni}^{\text{II}}(\text{L}^1)(\text{Cl})]^+$. Anal. calc. for $\text{C}_{14}\text{H}_{22}\text{Cl}_2\text{N}_4\text{NiO}_2$: C, 41.22; H, 5.44; N, 13.73 %. Found: C, 41.18; H, 5.51; N, 13.48 %. The synthesis of $[\text{Ni}(\text{L}^2)(\text{Cl})_2] \cdot \text{H}_2\text{O}$ (**2**) and $[\text{Cu}(\text{L}^2)(\text{ClO}_4)] \cdot \text{ClO}_4$ (**3**) is reported elsewhere.³¹ For complex **2**, ESI-MS in MeOH: $m/z^+ = 363.25$ for $[\text{Ni}^{\text{II}}(\text{L}^2)(\text{Cl})]^+$. Anal. calc. for $\text{C}_{16}\text{H}_{24}\text{Cl}_2\text{N}_4\text{NiO}$: C, 45.98; H, 5.79; N, 13.40 %. Found: C 46.20; H 5.74; N 13.83 %. For complex **3**, ESI in MeOH: $m/z^+ = 432.12$ for $[\text{Cu}^{\text{II}}(\text{L}^2)(\text{ClO}_4)]^+$. Anal. calc. for $\text{C}_{16}\text{H}_{22}\text{Cl}_2\text{CuN}_4\text{O}_8$: C, 36.07; H, 4.16; N, 10.52 %. Found: C, 36.31; H, 4.25; N, 10.48 %. Complex $[\text{Ni}(\text{L}^3)(\text{Cl})_2] \cdot \text{H}_2\text{O}$ (**4**) was prepared by adding the ligand L^3 (0.198 g; 0.512 mmol in 3 mL methanol) dropwise to a stirring solution of $[\text{Ni}^{\text{II}}(\text{H}_2\text{O})_6]\text{Cl}_2$ (0.122 g; 0.512 mmol) in methanol (5 mL). A dark green solution was obtained upon addition. The solution was stirred for 15 min at room temperature. Evaporation of solvent gave a dark green powder (yield: 91 %). For complex **4**, ESI-MS in MeOH: $m/z^+ = 479.33$ for $[\text{Ni}^{\text{II}}(\text{L}^3)(\text{Cl})]^+$. Anal. calc. for $\text{C}_{22}\text{H}_{36}\text{Cl}_2\text{N}_4\text{NiO}_3$: C, 49.47; H, 6.79; N, 10.49 %. Found: C, 49.36; H, 6.65; N, 10.77 %. Complex $[\text{Cu}(\text{L}^2)(\text{ClO}_4)] \cdot \text{ClO}_4 \cdot 2\text{H}_2\text{O}$ (**5**) was synthesized by adding ligand L^3 (0.20 g; 0.51 mmol in 3 mL methanol) dropwise to a solution of $[\text{Cu}^{\text{II}}(\text{H}_2\text{O})_6](\text{ClO}_4)_2$ (0.19 g; 0.51 mmol in methanol). The solution was stirred for 5 min at room temperature. A blue solid was obtained once the solvent was evaporated under vacuum (yield: 41 %). For complex **5**, ESI-MS in MeOH: $m/z^+ = 548.25$ for $[\text{Cu}^{\text{II}}(\text{L}^3)(\text{ClO}_4)]^+$. Anal. calc. for $\text{C}_{22}\text{H}_{34}\text{Cl}_2\text{CuN}_4\text{O}_{10}$: C, 38.58; H, 5.59; N, 8.18 %. Found: C, 38.51; H, 5.34; N, 8.09 %.

Caution: Although we have not experienced any issues, perchlorate salts are potentially explosive and should be handled in small quantities and with extreme care.

Electrochemistry and bulk electrolysis. The electrochemical behaviors of the complexes were investigated with a BAS 50W potentiostat/galvanostat. Cyclic voltammograms were obtained at room temperature in acetonitrile containing 0.1 M of *n*-Bu₄NPF₆ as the supporting electrolyte under argon atmosphere. The electrochemical cell employed three electrodes: glassy-carbon (working), platinum wire (auxiliary) and Ag/AgCl (reference). The ferrocene/ferrocenium redox couple Fc/Fc⁺ ($E^0 = 401$ mV NHE) was used as the internal reference. Peak to peak potential separations ($\Delta E_p = |E_{pc} - E_{pa}|$) and $|i_{pa} / i_{pc}|$ values were measured to evaluate the reversibility of the redox processes.

Catalysis. Electrocatalysis was performed in the custom-made air-tight H-type cell under inert conditions. The cell was comprised of two compartments separated by a frit. The working (mercury

pool) and reference (Ag/AgCl) electrodes were placed on one side of the frit, while the auxiliary electrode (coiled 12 inch Pt wire) was placed on the other side. During electrocatalysis, the cell was purged with N₂ gas for 10 min., followed by a sampling of the headspace gas (1 x 10⁻⁴ L) to ensure an O₂ free environment in the gas-chromatograph. For water reduction (phosphate buffer medium) 1 x 10⁻⁵ M of **1-5** was used; for proton reduction (acetonitrile medium), 5 x 10⁻⁶ mol of **1-5** was used. The volume of the phosphate buffer/acetonitrile used for electrocatalysis was 20 mL. The amount of hydrogen generated was determined in a Gow-Mac 400 gas chromatograph (GC) equipped with a thermal conductivity detector, and a 8 ft x 1/8 in., 5 Å molecular sieve column operating at a temperature of 60 °C. Nitrogen was used as a carrier gas at a flow rate of 30 mL.min⁻¹. The amount of H₂ produced was quantified using a calibration curve of mol of hydrogen versus peak area. Turnover numbers and the Faradaic efficiency of the metal complex were calculated from the amount of H₂ released and the charge consumed.

Computational Methods. Electronic structure calculations were carried out with the Gaussian 09 software package⁵² using B3LYP density functional.^{53,54} The SDD basis set and effective core potential⁵⁵ were used for Ni and Cu atoms and the 6-31G(d,p) basis set^{56,57} was used for the other atoms. Solvation effects in water were incorporated by using the implicit SMD solvation model⁵⁸ and were included during structure optimization. All the optimized structures were confirmed as minima by harmonic vibrational frequency calculations and the converged wave functions were tested for the SCF stability. The zero-point energy and thermal corrections were included for the calculation of the free energies. The standard states of 1 M concentration were considered for all the reactants and products for calculating the free energies of reactions. The calculation of the reduction potentials of the complexes included zero-point energy and thermal corrections and standard thermodynamic equation $\Delta G = -nFE$ was used. The calculated potentials were referenced to a value of E_{1/2} = 3.99 V for the ferrocene/ferrocenium couple calculated under our level of theory.

Photocatalysis. Samples for photocatalysis were prepared in 15 mL vials with gas-tight screw caps and septa. All samples were protected from light before use. The amounts of Ni catalyst and fluorescein were varied depending on the conditions used. The pH of the solutions was adjusted using NaOH and HCl as measured with a pH meter. The total volume of the samples was 10.0 mL. During the photocatalytic process, the cell was purged with N₂ gas for 5 min followed by a sampling of the headspace gas (1 x 10⁻⁴ L) to ensure an O₂ free environment in the gas-chromatograph. The amount of hydrogen generated was determined by a Gow-Mac 400 gas chromatograph. Nitrogen was used as the carrier gas at a flow rate of 30 mL/min. The amount of H₂ produced was quantified using a calibration curve of moles of hydrogen versus peak area. All of the photocatalytic samples were placed in a water jacketed cell at 20 °C for irradiation with green light (green light emitting diode at 520 nm). For the Hg poisoning test, the minimum required amount of mercury was used to inhibit the catalysts, and this result supports the presence of molecular catalysis.

Acknowledgments

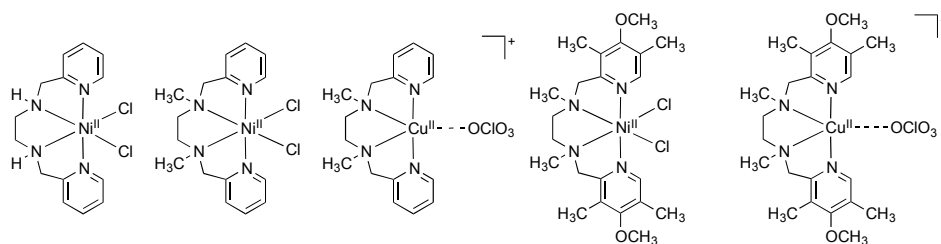
This work was supported by the Coordenação de Aperfeiçoamento de Pessoal de Nível Superior - Brazil (CAPES) - Finance Code 001 and the Conselho Nacional de Desenvolvimento Científico e Tecnológico - Brazil (CNPq 406593/2013-2 and 310768/2016-0) to M.L., the NFR and IIDR awards of the University of Alabama in Huntsville to A.M., the U.S. Department of Energy, Office of Science, Office of Basic Energy Sciences award DE-SC0001907 to C.N.V., and a New Faculty Seed Grant from IIT- Jammu, India to S.M.. M.L. acknowledges the Laboratório Multiusuário de Espectroscopia (LAME-UFF) and the Laboratório Multiusuário de Espectrometria de Massas (LAMEM-UFF). P.H.A.K. and D.M.E. acknowledge the WSU-Graduate School for support as Thomas C. Rumble Graduate Fellows.

Keywords: • copper • nickel • substituent effects • dihydrogen evolution, water reduction •

- 1 C. C. L. McCrory, C. Uyeda, J. C. Peters, *J. Am. Chem. Soc.* 2012, **134**, 3164-3170.
- 2 O. R. Luca, S. J. Konezny, J. D. Blakemore, D. M. Colosi, S. Saha, G. W. Brudvig, V. S. Batista, R. H. Crabtree, *New J. Chem.* 2012, **36**, 1149-1152.
- 3 P. Zhang, M. Wang, Y. Yang, D. Zheng, K. Han, L. Sun, *Chem. Commun.* 2014, **50**, 14153-14156.
- 4 Y. Sun, J. P. Bigi, N. A. Piro, M. L. Tang, J. R. Long, C. J. Chang, *J. Am. Chem. Soc.* 2011, **133**, 9212-9215.
- 5 Y. Na, M. Wang, K. Jin, R. Zhang, L. Sun, *J. Organomet. Chem.* 2006, **691**, 5045-5051.
- 6 R. Mejia-Rodriguez, D. Chong, J. H. Reibenspies, M. P. Soriaga, M. Y. Darensbourg, *J. Am. Chem. Soc.* 2004, **126**, 12004-12014.
- 7 Artero, V.; Fontecave, M. *Chem. Soc. Rev.* 2013, **42**, 2338
- 8 W. M. Singh, T. Baine, S. Kudo, S. Tian, X. A. N. Ma, H. Zhou, N. J. DeYonker, T. C. Pham, J. C. Bollinger, D. L. Baker, B. Yan, C. E. Webster, X. Zhao, *Angew. Chem. Int. Ed.* 2012, **51**, 5941-5944.
- 9 T. Fang, L.-Z. Fu, L.-L. Zhou, S.-Z. Zhan, S. Chen, *Electrochim. Acta* 2015, **178**, 368-373.
- 10 B. D. Stubbert, J. C. Peters, H. B. Gray, *J. Am. Chem. Soc.* 2011, **133**, 18070-18073.
- 11 D. Basu, S. Mazumder, X. Shi, H. Baydoun, J. Niklas, O. Poluektov, H. B. Schlegel, C. N. Verani, *Angew. Chem. Int. Ed.* 2015, **54**, 2105-2110.
- 12 D. Basu, S. Mazumder, X. Shi, H. Baydoun, J. Niklas, O. Poluektov, H. B. Schlegel, C. N. Verani, *Angew. Chem.* 2015, **127**, 2133-2138.
- 13 A. Call, Z. Codolà, F. Acuña-Parés, J. Lloret-Fillol, *Chem. Eur. J.* 2014, **20**, 6171-6183.
- 14 J. Han, W. Zhang, T. Zhou, X. Wang, R. Xu, *RSC Adv.* 2012, **2**, 8293-8296.
- 15 O. R. Luca, J. D. Blakemore, S. J. Konezny, J. M. Praetorius, T. J. Schmeier, G. B. Hunsinger, V. S. Batista, G. W. Brudvig, N. Hazari, R. H. Crabtree, *Inorg. Chem.* 2012, **51**, 8704-8709.
- 16 L.-Z. Fu, T. Fang, L.-L. Zhou, S.-Z. Zhan, *RSC Adv.* 2014, **4**, 53674-53680.
- 17 G. Wulfsberg, *Inorganic Chemistry*, University Science Books, Sausalito, 2000, pp.978.
- 18 R. Tatematsu, T. Inomata, T. Ozawa, H. Masuda, *Angew. Chem. Int. Ed.* 2016, **55**, 5100-5100.
- 19 P. Zhang, M. Wang, Y. Yang, T. Yao, L. Sun, *Angew. Chem. Int. Ed.* 2014, **53**, 13803-13807.
- 20 P. H. A. Kankanamalage, S. Mazumder, V. Tiwari, K. K. Kpogo, H. B. Schlegel, C. N. Verani, *Chem. Commun.* 2016, **52**, 13357-13360.
- 21 D. M. Ekanayake, K. M. Kulesa, J. Singh, K. K. Kpogo, S. Mazumder, H. B. Schlegel, C. N. Verani, *Dalton Trans.* 2017, **46**, 16812-16820.
- 22 Z. Han, L. Shen, W. W. Brennessel, P. L. Holland, R. Eisenberg, *J. Am. Chem. Soc.* 2013, **135**(39), 14659-14669.
- 23 M. L. Helm, M. P. Stewart, R. M. Bullock, M. R. DuBois, D. L. DuBois. *Science* 2011, **333**, 863-866.
- 24 J. Y. Yang, S. E. Smith, T. Liu, W. G. Dougherty, W. A. Hoffert, W. S. Kassel, M. R. DuBois, D. L. DuBois, R. M. Bullock. *J. Am. Chem. Soc.* 2013, **135**, 9700-9712.
- 25 [Z. Xin, S. Liu, C. Li, Y. Lei, D. Xue, X. Gao, H. Wang. *Int. J. Hydrog. Energy* 2017, **42**(7), 4202-4207.
- 26 J. Collin, A. Jouaiti, J. Sauvage. *Inorg. Chem.* 1988, **27**(11), 1986-1990.
- 27 P. Jacques, V. Artero, M. Fontecave. *PNAS* 2009, **106**(49), 20627-20632.
- 28 B. P. Yurkanis, *Organic Chemistry*, Pearson Education, New Jersey, 2001, pp. 637.
- 29 M Lanznaster, A. Neves, A. J. A. J. Bortoluzzi, A. M. C. Assumpcao, I. Vencato, S. P. Machado, S. M. Drechsel. *Inorg. Chem.* 2006, **45**, 1005-1011.
- 30 A. I. Francisco, M. D. Vargas, J. W. M. Carneiro, M. Lanznaster, J. C. Torres, C. A. Camara, A. C. Pinto. *J. Mol. Struct.* 2008, **891**, 228-232.
- 31 N. Singh, J. Niklas, O. Poluektov, K. M. Van Heuvelen, A. Mukherjee, *Inorg. Chim. Acta* 2017, **455**, 221-230.
- 32 R. N. Firmo, I. C. A. Souza, F. S. Miranda, C. B. Pinheiro, J. A. L. C. Resende, M. Lanznaster. *Polyhe.* 2016, **117**, 604-611.
- 33 C. Hureau, G. Blondin, M.-F. Charlot, C. Philouze, M. Nierlich, M. Césario, E. Anxolabéhère-Mallart, *Inorg. Chem.* 2005, **44**, 3669-3683.
- 34 M. S. Kryatova, O. V. Makhlynets, A. Y. Nazarenko, E. V. Rybak-Akimova, *Inorg. Chim. Acta* 2012, **387**, 74-80.
- 35 Zhou, J.; Zhu, B.-W.; Luan, J.; Liu, Z.; Fang, J.-K.; Bao, X.; Peng, G.; Tucek, J.; Bao, S.-S.; Zheng, L.-M. *Dalton Trans.* 2015, **44**, 20551-20561.
- 36 H. J. G. Hernández, T. Pandiyan, S. Bernes, *Inorg. Chim. Acta* 2006, **359**(1), 1-12.
- 37 S. Roeser, F. Bozoglian, C. J. Richmond, A. B. League, M. Z. Ertem, L. Francas, P. Miro, J. Benet-Buchholz, C. J. Cramer, A. Llobet, *Catal. Sci. Technol.* 2016, **6**, 5088-5101.
- 38 N. B. M. Posada, M. A. Guimarães, D. S. Padilha, J. A. L. C. Resende, R. B. Faria, M. Lanznaster, R. S. Amado, M. Scarpellini. *Polyhe.* 2018, **141**, 30-36.
- 39 L. Gan, T. L. Groy, P. Tarakeshwar, S. K. S. Mazinani, J. Shearer, V. Mujica, A. K. Jones, *J. Am. Chem. Soc.* 2015, **137**, 1109-1115.
- 40 U. J. Kilgore, J. A. S. Roberts, D. H. Pool, A. M. Appel, M. P. Stewart, M. R. DuBois, W. G. Dougherty, W. S. Kassel, R. M. Bullock, D. L. DuBois, *J. Am. Chem. Soc.* 2011, **133**, 5861-5872.
- 41 A. Zarkadoulas, M. J. Field, C. Papatrifiantafyllopoulou, J. Fize, V. Artero, C. A. Mitsopoulou, *Inorg. Chem.* 2016, **55**, 432-444.
- 42 D. C. Olson, J. Vasilevskis, *Inorg. Chem.* 1969, **8**, 1611-1621.
- 43 Y.-J. Sun, Q.-Q. Huang, J.-J. Zhang, *Inorg. Chem.* 2014, **53**, 2932-2942.
- 44 S. Mahapatra, N. Gupta, R. Mukherjee, *J. Chem. Soc., Dalton Trans.* 1991, **11**, 2911-2915.
- 45 S. Mahapatra, R. Mukherjee, *J. Chem. Soc., Dalton Trans.* 1992, **15**, 2337-2341.
- 46 W. Cañon-Mancisidor, E. Spodine, D. Venegas-Yazigi, D. Rojas, J. Manzur, S. Alvarez, *Inorg. Chem.* 2008, **47**, 3687-3692.
- 47 A. F. M. Silva, C. B. Pinheiro, J. A. L. C. Resende, M. Lanznaster. *Polyhe.* 2017, **123**, 132.
- 48 I. C. A. Souza, L. V. Faro, C. B. Pinheiro, D. T. G. Gonzaga, F. C. Silva, V. F. Ferreira, F. S. Miranda, M. Scarpellini, M. Lanznaster. *Dalton Trans.* 2016, **45**, 13671-13674.
- 49 F. L. S. Bustamante, F. S. Miranda, F. A. V. Castro, J. A. L. C. Resende, M. D. Pereira, M. Lanznaster. *J. Inorg. Biochem.* 2014, **132**, 37-44.
- 50 M. Wang, L. Chen, L. Sun, *Energ. Environ. Sci.* 2012, **5**, 6763-6778.
- 51 Z. Han, W. R. McNamara, M.-S. Eum, P. L. Holland, R. Eisenberg, *Angew. Chem. Int. Ed.* 2012, **51**, 1667-1670.
- 52 M. J. Frisch, G. W. T., H. B. Schlegel, G. E. Scuseria, M. A.; Robb, J. R. C., G. Scalmani, V. Barone, B. Mennucci, ; G. A. Petersson, H. N., M. Caricato, X. Li, H. P. Hratchian,; A. F. Izmaylov, J. B., G. Zheng, J. L. Sonenberg, M. Hada, ; M. Ehara, K. T., R. Fukuda, J. Hasegawa, M. Ishida, T.; Nakajima, Y. H., O. Kitao, H. Nakai, T. Vreven, J. A.; Montgomery, J., J. E. Peralta, F. Ogliaro, M. Bearpark, J. J. Heyd, E. B., K. N. Kudin, V. N. Staroverov, T. Keith, R.; Kobayashi, J. N., K. Raghavachari, A. Rendell, J. C.; Burant, S. S. I., J. Tomasi, M. Cossi, N. Rega, J. M. Millam, ; M. Klene, J. E. K., J. B. Cross, V. Bakken, C. Adamo, J.; Jaramillo, R. G., R. E. Stratmann, O. Yazyev, A. J. Austin,; R. Cammi, C. P., J. W. Ochterski, R. L. Martin, K.; Morokuma, V. G. Z., G. A. Voth, P. Salvador, J. J. ; Dannenberg, S. D., A. D. Daniels, O. Farkas, J. B.; Foresman, J. V. O., J. Cioslowski, and D. J. Fox, Gaussian 09, revision D.01. *Gaussian*, Inc. Wallingford, CT, 2013.
- 53 S. H. Vosko, L. Wilk, M. Nusair, *Can. J. Phys.* 1980, **58**, 1200-1211.
- 54 C. Lee, W. Yang, R. G. Parr, *Phys. Rev. B* 1988, **37**, 785-789.
- 55 M. Dolg, U. Wedig, H. Stoll, H. Preuss, *J. Chem. Phys.* 1987, **86**, 866-872.
- 56 P. C. Hariharan, J. A. Pople, *Theor. Chim. Acta* 1973, **28**, 213-222.

1
2 57 M. M. Francl, W. J. Pietro, W. J. Hehre, J. S. Binkley, M. S. Gordon, D. J. DeFrees, J. A. Pople, *J. Chem. Phys.* 1982, **77**, 3654-3665.
3 58 A. V. Marenich, C. J. Cramer, D. G. Truhlar, *J. Phys. Chem. B* 2009, **113**(18), 6378-6396.
4
5
6
7
8
9
10
11
12
13
14
15
16
17
18
19
20
21
22
23
24
25
26
27
28
29
30
31
32
33
34
35
36
37
38
39
40
41
42
43
44
45
46
47
48
49
50
51
52
53
54
55
56
57
58
59
60

The ligand substituents have a major effect on the redox potentials, catalytic efficiency and robustness of the complexes in HER



1
2
3
4
5
6
7
8
9
10
11
12
13
14
15
16
17
18
19
20
21
22
23
24
25
26
27
28
29
30
31
32
33
34
35
36
37
38
39
40
41
42
43
44
45
46
47
48
49
50
51
52
53
54
55
56
57
58
59
60